A MEMS-enabled 3D zinc–air microbattery with improved discharge characteristics based on a multilayer metallic substructure

2011 J. Micromech. Microeng. 21 104011

(http://iopscience.iop.org/0960-1317/21/10/104011)

J. Micromech. Microeng. **21** (2011) 104011 (6pp) doi:10.1088/0960-1317/21/10/104011

A MEMS-enabled 3D zinc–air microbattery with improved discharge characteristics based on a multilayer metallic substructure

A Armutlulu[1], Y Fang[1], S H Kim[2], C H Ji[3], S A Bidstrup Allen[1] and M G Allen[1,2]

[1] School of Chemical and Biomolecular Engineering, Georgia Institute of Technology, 311 Ferst Drive, Atlanta, GA 30332, USA
[2] School of Electrical and Computer Engineering, Georgia Institute of Technology, 791 Atlantic Drive, Atlanta, GA 30332, USA
[3] Department of Electronics Engineering, College of Engineering, Ewha Womans University, Seoul 120-750, Korea

E-mail: aarmutlulu3@gatech.edu

Received 2 April 2011, in final form 17 June 2011
Published 29 September 2011
Online at stacks.iop.org/JMM/21/104011

Abstract
This paper reports the design, fabrication and testing of a three-dimensional zinc–air microbattery with improved areal energy density and areal capacity, particularly at high discharge rates. The device is based on a multilayer, micron-scale, low-resistance metallic skeleton with an improved surface area. This skeleton consists of alternating Cu and Ni layers supporting Zn as electrodeposited anode electrode, and provides a high surface area, low-resistance path for electron transfer. A proof-of-concept zinc–air microbattery based on this technology was developed, characterized and compared with its two-dimensional thin-film counterparts fabricated on the same footprint area with equal amount of the Zn anode electrode. Using this approach, we were able to improve a single-layer initial structure with a surface area of 1.3 mm^2 to a scaffold structure with ten layers having a surface area of 15 mm^2. Discharging through load resistances ranging from 100 to 3000 Ω, the areal energy density and areal capacity of the microbattery were measured as 2.5–3 mWh cm^{-2} and ∼2.5 mAh cm^{-2}, respectively.

(Some figures in this article are in colour only in the electronic version)

1. Introduction

The miniaturization of electromechanical systems via microfabrication technologies has led to an increase in demand for the similarly scaled energy storage devices that, although small, power these highly functional systems. Even though there has been enormous progress in the development of microdevices, such as autonomous microactuators and microsensors for implantable microsystems, the development of compatible and miniaturized power sources remains elusive. Batteries with high energy storage capability and power density are an attractive microsystem power solution [1]. To maximize the performance of the batteries in microdevices with limited available area or small footprints onboard, microbatteries with three-dimensional (3D) architecture as opposed to two-dimensional (2D) thin-film battery electrodes are needed, for example incorporating high aspect ratio electrode structures for the maximum surface area [2, 3].

Due to their high energy densities resulting mainly from the usage of atmospheric oxygen as one of the electrodes, zinc–air batteries are good candidates for the previously mentioned miniaturized applications. Commercially available zinc–air batteries utilize Zn powder for the anode electrode, achieving high surface area as well as high energy density [4].

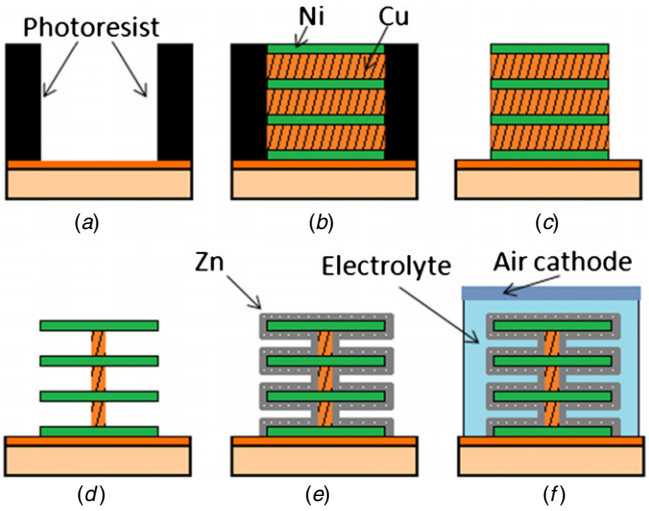

Figure 1. Schematic description of the fabrication process in six steps: (*a*) deposition and patterning of photoresist, (*b*) electrodeposition of alternating Ni and Cu layers, (*c*) removal of photoresist, (*d*) partial etching of sacrificial Cu layers, (*e*) electrodeposition of the Zn layer and (*f*) injection of electrolyte into the case surrounding the battery and sealing the top with the air cathode.

However, it has been recently shown that especially at high discharge rates, zinc oxide formation on the anode surface over time results in an increase in the internal resistance that limits the discharge rate of the battery and thus decreases its performance [5]. In order to maintain the inherent high energy density and improve the discharge characteristics of the zinc–air battery, microfabricated zinc–air batteries with well-ordered 3D Zn pillar microstructures for high surface area and reduced internal resistance have been demonstrated [5, 6].

The work reported herein focuses on the development of 3D Zn anode structures coated on a highly laminated metallic substructure 'skeleton', based on a sequential multilayer robotic electroplating process [7]. The mechanically rigid and conductive metallic skeleton with multiple parallel layers provides an enhanced electrode surface area accessible to the electrolyte which is essential for high discharge rates. The lateral surface approach allows for higher aspect ratios than the vertically oriented pillar structures reported previously. In addition, the electrochemically inert conducting skeleton supporting the Zn electrode enables continuous and consistent electrical access to every region on its surface where Zn is available and thus yields improved discharge characteristics. In order to demonstrate the advantages of this approach, both 2D thin-film and 3D laminated substructure microbatteries are fabricated and their performance is compared.

2. Development of the 2D and 3D zinc–air microbatteries

2.1. Fabrication of the metallic skeleton

The fabrication process of the proposed zinc–air microbattery is schematically shown in figure 1. Seed layers of Ti/Cu/Ti were sputtered onto a thermally oxidized silicon wafer. The top Ti seed layer was spin-coated with a negative tone photoresist (NR21-2000P, Futurrex) that formed a film having an approximate thickness of 60 μm. This photoresist film was shaped in a prescribed pattern via UV lithography to be utilized as a high aspect ratio electroplating mold for the metallic skeleton structures with alternating Ni and Cu layers. Once the mold was prepared, the exposed top Ti seed layer was removed using diluted HF. The underlying Cu layer was utilized as a seed layer for the sequential robotic electroplating-based-lamination skeleton [7]. In this process, multiple layers of Ni and Cu were alternately electroplated at a constant current density of 10 mA cm^{-2}. A sulfate-based Ni plating bath and a commercial Cu plating bath were utilized for the repetitive alternating deposition of structural Ni and sacrificial Cu layers, respectively [8]. Following the electroplating process, the photoresist mold was removed via acetone.

Figure 2 illustrates the structures immediately after removal of the mold. The etching holes labeled in figure 2(*b*) refer to those areas that were occupied by the photoresist mold during the electroplating process. They are vertically separated from each other by air bridges that have a width of 15 μm. After the removal of the mold, these holes provide additional regions for the etchant to dissolve the interlayer Cu. The Cu layers were partially and selectively etched via a timed wet etching process based on an ammonium hydroxide/copper sulfate etchant. The experimentally determined etching rate at room temperature was found to be approximately 0.6 μm min^{-1}. Following a 20 min etching process, all the Cu between vertically adjacent air bridges were completely etched away and a controlled amount of undercut was formed in the vicinity of the etching holes. This process resulted in the formation of Ni air bridges, as seen in figure 3(*a*). The interlayer mechanical support, as well as the interlayer electrical connection, was provided by the Cu remaining between the horizontally adjacent etching holes.

Estimating the Cu etching rate is a crucial step since it plays a key role in determining the surface area of the structure. The more Cu is etched, the more surface area is exposed that can ultimately be coated by Zn. However, it is also important to preserve a certain amount of Cu to provide both mechanical support and electrical connectivity between the parallel Ni layers. Hence, the Cu etching should be well optimized so that the remaining Cu layers are narrow enough to provide as much surface area as possible and thick enough to prevent any Ni layers from delaminating. In order to avoid collapsing of the air bridges during drying, the structure is immersed in a series of liquids in the following order: DI water—isopropyl alcohol—methanol where each following liquid has lower capillary forces than its predecessor, prior to full drying [9].

Based on the above process, proof-of-concept structures with ten pairs of Ni/Cu layers were fabricated. Individual layer thicknesses of Ni and Cu were approximately 2 and 4 μm, respectively. After the partial removal of the sacrificial Cu layers, the metallic skeleton had a surface area that is seven times greater than that of its footprint. Theoretically,

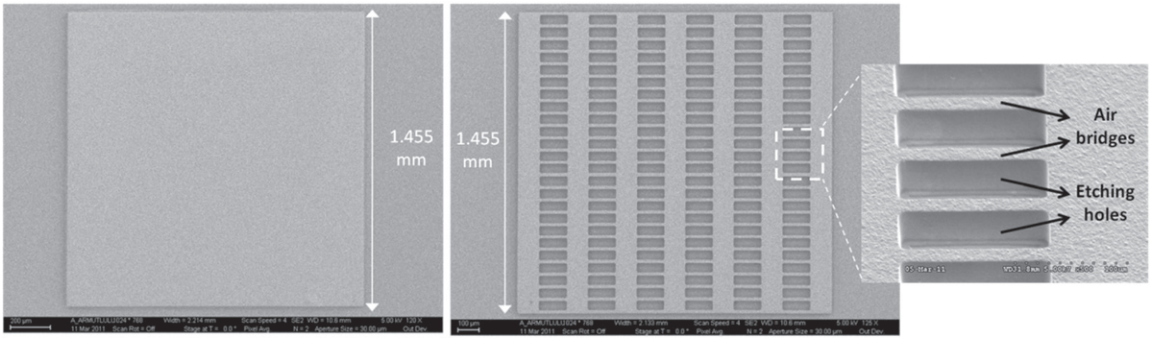

(*a*) (*b*)

Figure 2. SEM image of the top view of the metallic skeletons right after photoresist removal: (*a*) unpatterned structure (*b*) patterned structure with etching holes and air bridges.

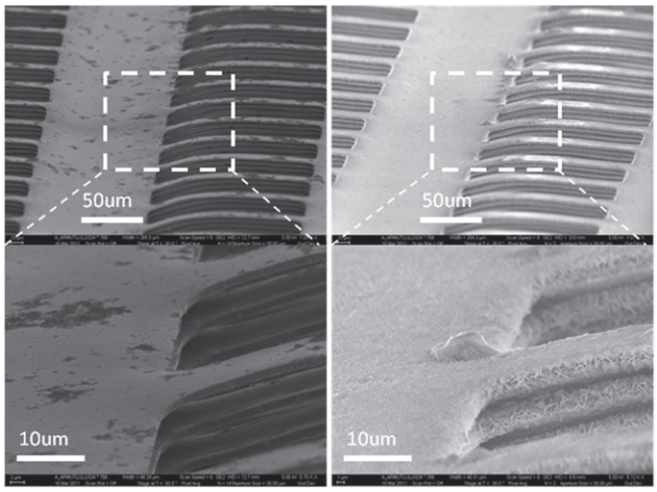

(*a*) (*b*)

Figure 3. SEM images of the metallic skeleton substructure (*a*) after partial removal of sacrificial Cu layers, (*b*) after Zn electrodeposition.

it is possible to increase the surface area by more than two orders of magnitude provided that there is a sufficient number of layers. In addition to increased number of layers, structures with higher surface areas could also be achieved by modifying the geometry of the etching holes.

2.2. *Fabrication of the anode electrode*

The anode fabrication process involves electrodeposition of Zn onto the metallic skeleton. Zn was electroplated at a constant current density of approximately 10 A dm^{-2} utilizing an acid chloride Zn electroplating bath [8]. Immediately prior to the electroplating process, a vacuum treatment was applied in order to ensure the removal of the trapped air in the etching holes and in between the Ni layers to enable the diffusion of the plating bath to the available surface on the metallic skeleton. This approach to complete coverage not only most efficiently utilizes the available electrode area, but also reduces the possibility of any potentially undesirable electrochemical reactions attributable to other metals being exposed to the electrolyte. Figure 3 shows the SEM images of the metallic skeleton before and after the Zn electrodeposition process. In order for the gap between two Ni layers (e.g. air bridges) to be maintained and thus to preserve the high surface area, it is important to control the electroplated Zn thickness. As can be seen in figure 3(*b*), a conformal Zn layer exists on the metallic skeleton surface while the clearance between two adjacent Ni layers persists after the plating process. The estimated thickness of the deposited Zn layer was approximately 1.5 μm.

In order to demonstrate the performance improvement provided by the metallic skeleton approach, the same amount of Zn was electroplated under the same plating conditions as before on an unpatterned and unetched Ni structure with the same footprint area and overall thickness as the aforementioned metallic skeleton as shown in figure 2(*a*). The reason for having a backbone structure for this thin-film Zn electrode is mainly to eliminate any performance discrepancies that may stem from the usage of different material as a current collector or from the difference in the total height of the structure. For further performance comparison, another thin-film anode electrode was fabricated by electroplating the same amount of Zn on an unpatterned Ti sheet with the same footprint area but without any backbone structure. The discharge performances of these three batteries are discussed and compared below.

2.3. *Assembly of the zinc–air microbattery*

The final form of the zinc–air microbattery is depicted schematically in figure 1(*f*). The anode structure, surrounded by an epoxy case that contains the electrolyte, was assembled with a commercially available air cathode (E4A with separator, Electric Fuel) consisting of three major layers [10]. The top blocking layer comprises a laminated porous Teflon film that allows oxygen to diffuse in and prevents the battery from leaking electrolyte. The median layer contains the active cathode material which is manganese-based catalyzed carbon supported by a woven Ni mesh. To complete the circuit in the testing stage, a copper wire is soldered to the edge of this Ni mesh after cleaning off the carbon. The bottom layer facing the electrolyte serves as a separator layer composed of a laminate of a polypropylene microporous film with a thin polypropylene non-woven that is made hydrophilic with a

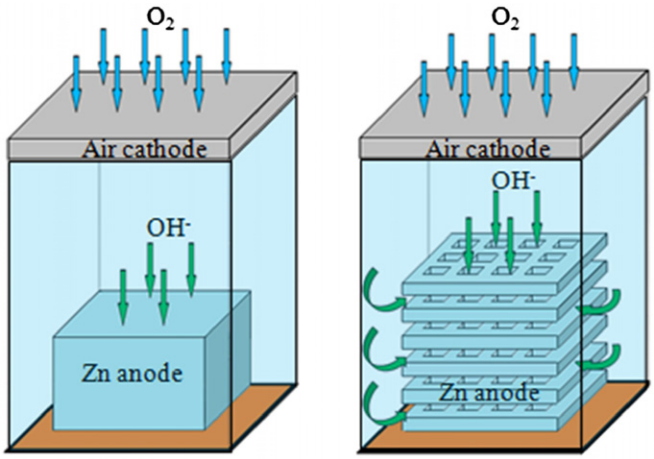

Figure 4. Schematic comparison of the air access in thin-film and multilayer batteries.

surfactant. This layer acts as an insulator between the anode and the cathode while allowing flow of ions in the electrolyte. Once the soldering was completed, the cut edges of the air cathode were sealed with epoxy. The cathode area is important in the sense that it regulates the oxygen transfer to the electrolyte. For the sake of consistency, air cathodes with the same surface area were utilized for both thin-film and multilayer batteries.

A 7 M aqueous KOH solution was utilized as the battery electrolyte. The electrolyte was injected into the case surrounding the anode following a vacuum treatment. As in the case of the Zn plating process, this treatment ensures the removal of the air trapped deep in between the laminated layers and thus provides substantial contact between the electrolyte and the entire Zn anode surface.

Figure 4 illustrates the air access to thin-film and multilayer batteries. The catalyzed carbon in the air cathode causes the oxygen-reduction half-cell reaction which results in the production of hydroxide ions. These ions migrate to the anode and react with Zn forming soluble zincate ions which eventually precipitate to form zinc oxide as the discharge proceeds.

3. Investigation of the discharge characteristics of the zinc–air microbattery

Proof-of-concept zinc–air microbatteries with ten layers were tested by discharging under five different electrical loads having resistance values of 100, 250, 500, 1000 and 3000 Ω, respectively. The discharge profiles of the latter four are shown in figure 5. Similarly, thin-film zinc–air batteries built on Ni backbone and Ti layer sheet were also discharged under the same loads. During the discharge tests, voltage values were simultaneously measured and recorded with respect to time using LabVIEW software (SignalExpress). A close view of the etching holes immediately after the discharge can be seen in figure 6. It is apparent that the metallic skeleton remains intact throughout the discharge process.

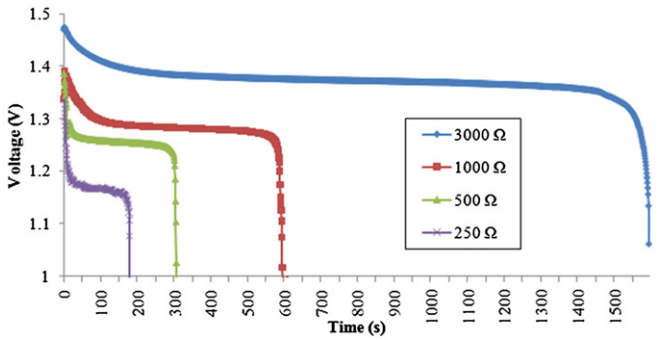

Figure 5. Discharge profile of the ten-layer zinc–air microbattery under four different electrical loads.

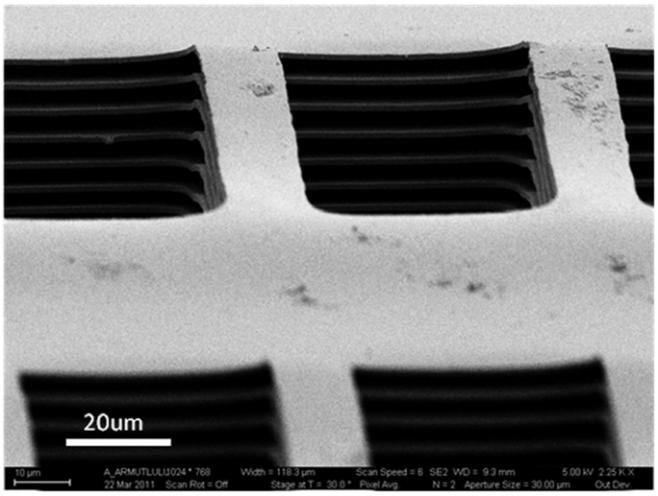

Figure 6. Close-up view of the etching holes of the metallic skeleton after discharge.

3.1. Evaluation of the battery performance

As can be seen in figure 5, discharge curves of the ten-layer microbatteries maintain a relatively flat voltage profile both at high and low discharge rates, with a small voltage decrease immediately after start-up, and a sharp voltage decrease near total discharge, which is typical for the discharge characteristics of zinc–air batteries. These discharge data were also used to calculate the areal capacity, Q_A, and areal energy density, E_A, of the microbatteries. To determine the areal capacity, discharge current, I_d, was integrated over time, t, and divided by the footprint area, A. The areal capacity was then multiplied by the average discharge voltage, V_{av}, to give the areal energy density:

$$Q_A = \int \frac{I_d \, \mathrm{d}t}{A} \tag{1}$$

$$E_A = Q_A \cdot V_{\text{av}}. \tag{2}$$

The comparison of the areal energy densities of different battery structures at varying discharge rates is shown in figure 7. The ten-layer zinc–air microbattery possesses higher areal energy densities than its thin-film counterparts at every measured discharge rate. The difference between these structures increases further as the discharge rate is increased.

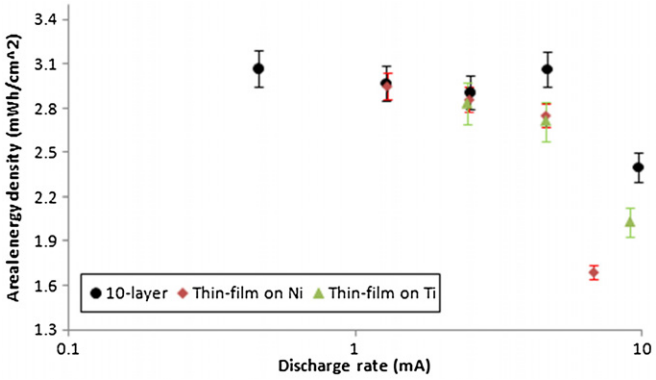

Figure 7. Comparison of areal energy densities of three different batteries as a function of discharge rates.

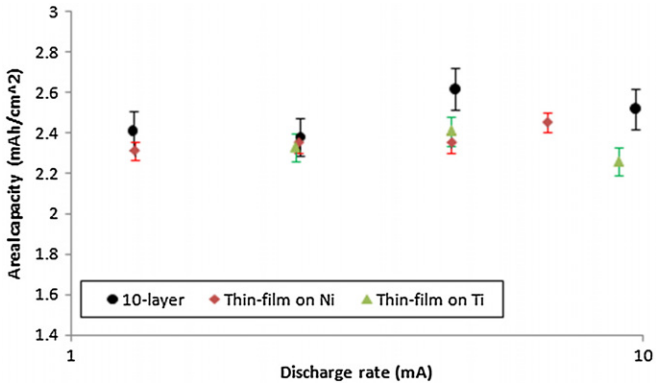

Figure 8. Comparison of areal capacities of three different batteries as a function of discharge rates.

In addition, the ten-layer microbattery maintains its high areal energy density of >3 mWh cm^{-2} until a discharge current of approximately 5 mA. In contrast, a decreasing trend is observed in the energy densities of thin-film microbatteries as the discharge rate is increased and then the areal energy density drops dramatically around 10 mA of discharge current. A similar decreasing trend of the energy densities has recently been reported for the commercial zinc–air batteries as well, where the anode electrode is made of zinc powder [5]. Areal capacities of these batteries are illustrated and compared in figure 8 as a function of discharge rate. As in the previous case, the ten-layer microbattery shows the best performance among all tested batteries, retaining its high capacity for every measured discharge rate.

As discussed in the fabrication section, the anode has been formed by electroplating Zn at 10 A dm^{-2} for 1 min which corresponds to a Zn mass of approximately 0.3 mg per structure. Based on this and the discharge data shown in figure 5, on average, 88% of the Zn deposited on the multilayer structure has been reacted during the discharge tests, whereas the percentage falls to 85% in the case of the thin-film battery.

These comparisons of the batteries which contain equal amount of Zn in their anode electrode built on the same footprint area support the fact that increasing the surface area is a substantial factor in improving the areal energy density and the areal capacity of the batteries, particularly at high discharge rates. Hence, to some extent, it is possible to achieve even higher energy densities and capacities via further improvement of the surface by increasing the number of layers in the metallic skeleton. For a height constrained structure, there might be a limit to the number of layers at some point due to the uneven current distribution and/or spacing between the layers which can be investigated via further experiments.

4. Summary

A proof-of-concept 3D zinc–air microbattery with a micromachined metallic scaffold supporting electrodeposited Zn anode electrode has been successfully developed, fabricated and tested along with thin-film microbatteries of the same footprint area with and without any backbone structure. Despite the fact that each of them had the same amount of Zn in their anode electrodes, based on the discharge test results, the ten-layer zinc–air microbattery was shown to be superior to its thin-film counterparts in terms of both areal energy and power densities, as well as areal capacities. The metallic scaffold approach provided a high surface area that is crucial for high discharge rates while maintaining consistent and continuous electrical access to the Zn anode electrode with a minimum ohmic loss. The energy density could be increased even by an order of magnitude by increasing the number of layers in the skeleton. This metallic skeleton approach might also be incorporated into other battery systems including secondary zinc–air batteries where a low-resistance scaffold structure might be required that is capable of providing high surface area as well as remaining intact throughout the discharge/charge cycles.

Acknowledgments

The authors would like to thank Richard Shafer and William Preston Galle for their help on the operation of the electroplating robot.

References

[1] Song J, Yang X, Zeng S S, Cai M Z, Zhang L T, Dong Q F, Zheng M S, Wu S T and Wu Q H 2009 Solid-state microscale lithium batteries prepared with microfabrication processes *J. Micromech. Microeng.* **19** 045004

[2] Harb J N, LaFollette R M, Selfridge R H and Howell L L 2002 Microbatteries for self-sustained hybrid micropower supplies *J. Power Sources* **104** 46–51

[3] Long J W, Dunn B, Rolison D R and White H S 2004 Three-dimensional battery architectures *Chem. Rev.* **104** 4463–92

[4] Vincent C A and Scrosati B 1997 *Modern Batteries: An Introduction to Electrochemical Power Sources* (Burlington, MA: Butterworth-Heinemann) p 100

[5] Chamran F, Min H S, Dunn B and Kim C J 2007 Zinc-air microbattery with electrode array of zinc microposts *Proc. IEEE Int. Conf. MEMS 2007 (Kobe, Japan)* pp 871–4

[6] Dunn B, Long J W and Rolison D R 2008 Rethinking multifunction in three dimensions for miniaturizing electrical energy storage *ECS Interface* **17** 49–53

[7] Galle W P, Kim S H, Shah U and Allen M G 2010 Micromachined capacitors based on sequential multilayer electroplating *Proc. IEEE Int. Conf. MEMS 2010 (Wanchai, Hong Kong)* pp 332–5

[8] Schlesinger M and Paunovic M 2000 *Modern Electroplating* (New York: Wiley-Interscience) 430–2

[9] Matovic J 2006 Application of Ni electroplating techniques towards stress-free microelectromechanical system-based sensors and actuators *Proc. Inst. Mech. Eng.* **220** 1645–54

[10] Linden D and Reddy T B 2001 *Handbook of Batteries* (New York: McGraw-Hill) p 38.5